OXFORD

International Journal of Neuropsychopharmacology (2020) 23(7): 459–468

doi:10.1093/ijnp/pyaa022
Regular Research Article

REGULAR RESEARCH ARTICLE

Aberrant Auditory Steady-State Response of Awake Mice After Single Application of the NMDA Receptor Antagonist MK-801 Into the Medial Geniculate Body

Xuejiao Wang, Yingzhuo Li, Jingyu Chen, Zijie Li, Jinhong Li, Ling Qin

Department of Physiology, China Medical University, Shenyang, People's Republic of China.

Correspondence: Ling Qin, MD, PhD, Department of Physiology, China Medical University, Shenyang, 110122, People's Republic of China (lqin@cmu.edu.cn).

Abstract

Background: Systemic administration of noncompetitive N-methyl-D-aspartate receptor (NMDAR) antagonists such as MK-801 is widely used to model psychosis of schizophrenia (SZ). Acute systemic MK-801 in rodents caused an increase of the auditory steady-state responses (ASSRs), the oscillatory neural responses to periodic auditory stimulation, while most studies in patients with SZ reported a decrease of ASSRs. This inconsistency may be attributable to the comprehensive effects of systemic administration of MK-801. Here, we examined how the ASSR is affected by selectively blocking NMDAR in the thalamus.

Methods: We implanted multiple electrodes in the auditory cortex (AC) and prefrontal cortex to simultaneously record the local field potential and spike activity (SA) of multiple sites from awake mice. Click-trains at a 40-Hz repetition rate were used to evoke the ASSR. We compared the mean trial power and phase-locking factor and the firing rate of SA before and after microinjection of MK-801 (1.5 μg) into the medial geniculate body (MGB).

Results: We found that both the AC and prefrontal cortex showed a transient local field potential response at the onset of click-train stimulus, which was less affected by the application of MK-801 in the MGB. Following the onset response, the AC also showed a response continuing throughout the stimulus period, corresponding to the ASSR, which was suppressed by the application of MK-801.

Conclusion: Our data suggest that the MGB is one of the generators of ASSR, and NMDAR hypofunction in the thalamocortical projection may account for the ASSR deficits in SZ.

Key Words: Local field potential, NMDAR, thalamus, prefrontal cortex, auditory cortex, psychosis

Introduction

The auditory steady-state responses (ASSRs) are evoked oscillatory responses that are entrained to the frequency and phase of repeating auditory stimulation (Picton et al., 2003). The ASSRs reflect the propensity of neurons to oscillate at a particular gamma-band "resonant" frequency induced by external periodic stimulation. Electroencephalographic and magnetoencephalographic recordings can be used to noninvasively detect ASSRs in humans, which show a peak frequency at 40 Hz (Pastor et al., 2002). A number of studies on the 40-Hz ASSR have reported reductions in the evoked power and phase-locking measures (i.e., inter-trial phase coherence) in individuals with schizophrenia (SZ) (Thune et al., 2016; Tada et al., 2019). The reduction of 40-Hz ASSR has been proposed as a biomarker of the N-methyl-D-aspartate receptor (NMDAR) hypofunction in SZ patients (Sivarao et al., 2016). Because administration of drugs that block NMDAR can mimic

Received: December 4, 2019; **Revised:** March 18, 2020; **Accepted:** March 21, 2020

Significance Statement

The auditory steady-state response (ASSR) is a well-used electrophysiological approach for examining the synchronizing responses from large ensembles of neurons and binding neural activity across brain areas. The deficits of ASSR may reflect the hypofunction of N-methyl-D-aspartate receptor (NMDAR), which is hypothesized to contribute to the pathophysiology of schizophrenia (SZ). In this way, NMDAR antagonists have been systemically applied in rodents to test whether alterations in NMDAR function produce ASSR disturbances similar to those observed in patients with SZ. However, the results of animal experiments are inconsistent. To avoid the comprehensive effects of systemic application of NMDAR antagonist, in this study, we examined whether NMDAR antagonist action in the thalamus can induce abnormal ASSR. We found evidence supporting that the medial geniculate body contributes to the generation of ASSR, and NMDAR hypofunction is associated with the reduction of ASSR. Our paradigms thus provide a powerful translational model for testing cellular mechanism of NMDAR dysfunction.

some aspects of synaptic dysfunction in SZ (Umbricht et al., 2000; Kirov et al., 2012; Timms et al., 2013), evaluating the 40-Hz ASSR in the animal models has been represented as a promising target in translational research (McNally et al., 2016). By recording electroencephalographic signals from the electrodes implanted in the brain of rodents, previous studies have established several measures to investigate the 40-Hz ASSR in the NMDAR hypofunction models induced by actually or chronically injecting NMDAR antagonists (Vohs et al., 2012; Hiyoshi et al., 2014; Leishman et al., 2015; Sullivan et al., 2015; Kozono et al., 2019). However, they commonly reported that the treatment of NMDAR antagonist causes an enhancement of 40-Hz ASSR, which is inconsistent with the frequently reported reduction of 40-Hz ASSR in SZ patients. Such an inconsistence may be attributable to the complicated effects of systemic application of NMDAR antagonist, which cannot specifically target the neural circuits of ASSR generation. Therefore, it is important to select a more specific approach to examine the association between NMDAR hypofunction and the ASSR deficits.

As for the generator of the 40-Hz ASSR, we have found the evidence supporting the auditory cortex (AC) as the region of ASSR originator by simultaneous recording from the electrodes directly implanted in multiple brain areas (Wang et al., 2018). Previous studies on humans also have localized the source of ASSR at the AC and the medial geniculate body (MGB) (Gutschalk et al., 1999; Herdman et al., 2002). The AC is the core station of cortical auditory processing, which plays a key role in the representation and perception of periodic sound stimulation (Bendor et al., 2010; Dong et al., 2011, 2013). The MGB is the auditory part of the thalamus, which provides the immediate inputs to the AC. The extensive afferent and efferent projections between the MGB and the AC constitute the primary neural circuit for auditory perception (Malmierca, 2003). Noninvasive neuroimaging studies in humans have revealed hyper-connectivity (i.e., greater correlation) between thalamus and cortical areas in SZ (Woodward et al., 2012; Anticevic et al., 2014; Klingner et al., 2014; Giraldo-Chica et al., 2017). The abnormality of thalamocortical connectivity can be observed before psychosis onset in at-risk patients (Anticevic et al., 2015). For this, the MGB is an appropriate candidate for the study of the neural mechanisms underlying ASSR deficits. In this study, we aimed to investigate the link between the 40-Hz ASSR deficits and NMDAR hypofunction in MGB. This was done by examining how the 40-Hz ASSRs are altered by direct administration of MK-801, an NMDAR antagonist known to produce ASSR changes in rodents (Hiyoshi et al., 2014), into the MGB of awake mice. Because prefrontal cortex (PFC) is also reported to be the target of systemic injection of NMDAR antagonists in animal models of SZ (Stefani et al., 2005; Blot et al., 2013, 2015), we simultaneously recorded the ASSRs in AC and PFC through the electrodes implanted in multi brain sites. And because ASSR is heavily affected by anesthesia (Wang et al., 2018), this study was conducted on unanesthetized mice.

METHODS

Animals

Six- to 8 week-old C57BL/6 mice (Vital River Laboratory, Beijing, China) were housed on a 12-hour-day/-night cycle to maintain their normal biorhythms and had free access to food and water. The animals were maintained and treated in compliance with the policies and procedures detailed in the "Guide for the Care and Use of Laboratory Animals" of the National Institutes of Health. All procedures were approved by the Animal Ethics Committee of China Medical University (no. KT2018060). Effort was made to minimize the suffering and discomfort of animals and to reduce the number of animals used.

Surgical Procedures

Mice were anesthetized with systemic injection of urethane (1.6 g/kg, i.p.) and with 2% lidocaine under the scalp. Body temperature was monitored rectally and maintained at 37°C using a feedback-controlled heating pad. Anesthetized mice were placed in a stereotaxic apparatus with blunt ear bars (#68001, RWD Life science, Shenzhen, China). Microelectrode arrays were implanted in the AC to record LFP and extracellular spike activities. Arrays consisted of eight 50-μm-diameter Teflon-coated tungsten micro wires (50 μm out diameter, #795500, A-M Systems, Sequim, WA) arranged in a 2×2 pattern measuring about 0.3×0.3 mm. Electrode arrays were implanted in the surface layer of AC (AP −3.0 mm, ML 4.0 mm, 0.3–0.5 mm below the dura). To record LFPs of the PFC, a stainless-steel screw electrode connected with a Teflon-coated sliver microwire (#785500, A-M Systems) was implanted over the left hemisphere skull of the PFC (AP = +1.8 mm, ML = 0.30 mm). The micro wires were soldered to a pin connector, which was secured onto the cranium of the right hemisphere using dental acrylic resin. A stainless-steel screw electrode over the cerebellum served as ground. To inject MK-801 into the MGB, a cannula (#62001; RWD Life Science) was implanted into the region of the left MGB (AP = −3.3 mm, ML = 2.0 mm, DV = 3.0 mm). Four additional skull screws were implanted serving as anchors.

Acoustic Stimuli

Click-trains were trains of rectangular pulses of a 0.2-millisecond duration each, which repeated at a rate of 40 cycles/s and continued for a total duration of 0.5 seconds. The waveforms of

sound stimuli were generated digitally with a 100-kHz sampling rate using a custom built MATLAB (Mathworks, Natick, MA) program and transferred to a analog signal by a D/A board (PCI-6052E, National Instruments, Austin, TX) then played through an open-field loudspeaker (K701, AKG, Vienna, Austria) placed at the top of a recording box. The intensity of the sound stimulus was adjusted to be at 70 dB SPL and measured at the center of the recording box (type 2238 sound level meter, Bruel & Kjær, Naerum, Denmark).

Electrophysiological Recording and MK-801 Infusion

Animals were allowed 1 week to recover from surgery before the start of experiments. After that, animals were acclimated to the sound-attenuated recording room. Briefly, the animals were transported in their home cage to the recording room where they were left alone for 5 minutes. They were then put in a mesh box (20×20×20 cm) and tethered to the recording system via a flexible cable and allowed to freely behave in the recording box for 15 minutes. This procedure was repeated for 3 days. Recording experiments started from the fourth day. A multi-channel preamplifier (PBX Preamplifier; Plexon, Dallas, TX) and a digital multichannel acquisition processor (Plexon) were used for signal filtering (1–300 Hz for LFP signal, 0.3–5 kHz for spike signal), amplification, and data acquisition. Multi-unit spikes were detected online by threshold crossing. LFPs were stored on a hard disk and then imported to MATLAB (The MathWorks) for the online averaging and monitoring of neural responses to sound stimuli.

In 1 recording session, 120 trials of click-trains were presented at random intervals between 4 and 8 seconds. After completing 1 session of recording under normal conditions, the mouse was restrained in a plastic tube and received a microinjection of 1.5 μg MK-801 (Sigma, dissolved in saline containing 5% DMSO at 3 μg/μL) or vehicle solution through stainless-steel tubes (30G) inserted into the MGB (AP = −3.0 mm, ML = 2.0 mm, DV = 3.0 mm). Solutions were delivered at a rate of 250 nL/min via a PE pipe (# 62302, RWD Life Science) connecting to a 10-μL Harvard Apparatus syringe pump system (Pump 11 Elite). The pipe was left in place for another 5 minutes at the end of injection and the cannulae capped to prevent reflux of the injected solution. The mouse was then released; the second recording session was conducted at 30 minutes after injection. Then, the animals were returned to their feeding cage. The recording and injection procedures were repeated 48 hours later. The mice injected with MK-801 in the first test round now received injection of vehicle and vice versa. Each mouse experienced 4 rounds of experiments with an interval of 1 day; MK-801 and vehicle were injected alternatively. Because the injection order had no effect on the results, the data of the 2 groups were pooled together for the presentation.

Analysis of LFP Data

Spectral analysis was conducted on the click-train evoked LFPs. LFPs were analyzed using a wavelet-based analysis algorithm implemented in custom-written code using eeglab toolbox (https://sccn.ucsd.edu/eeglab/index.php). Prior to spectral analysis, the LFP signals were visually inspected, referring to the video recordings of animal behavior, and the noisy trials containing the artifacts of abrupt movement were removed. If the percentage of noisy trial was beyond 5%, the whole session of data was discarded to ensure our data represented the animal's quiet state. There was no drug-related difference in the number of discarded sessions. The trial-based spectra of LFPs were accessed by the mean trial power (MTP) and phase-locking factor (PLF) analysis (Delorme et al., 2004). MTP was computed by averaging the LFP power in the spectral-temporal domain across the 120 trials from 1 session. PLF measures the synchronization of the LFP phase across individual trials at particular frequencies and time intervals. For the data recorded from 1 session, the MTP and PLF were calculated to obtain a spectral-temporal function using the multitaper method provided by eeglab. The results of MTP were presented following a dB baseline correction implemented by eeglab.

Analysis of Spike Activity

We computed the instantaneous firing rate from multi-unit spike activity for each stimulus presentation, which were used to construct peri-stimulus time histograms (PSTHs) and raster plots from −500 to 1000 milliseconds relative to the onset of stimulus. This was accomplished using 1-millisecond bins for each stimulus trial; each 1-millisecond bin contained 1 or 0 timestamps representing the discharges from the unit as a series of zeros and ones across the analysis window that was displayed as a raster plot. Then, each column of this matrix was smoothed with a 5-millisecond Gaussian sliding window, which transformed each binned vector of zeros and ones into a continuous waveform that represents the instantaneous firing rate of each trial for each unit.

Histology

To confirm the position of the electrodes, at the end of the experimental period, all animals were deeply anesthetized with pentobarbital (100 mg/kg). The animals were then perfused transcardially with fixative (4% paraformaldehyde). The brains were removed and placed in fixative solution. After further fixation, the brains were coronal sectioned in 40-mm slices, collected on noncoated glass slides, and stained with thinonin. Electrode tip positions were confirmed by microscopic observation of the slides.

Statistical Analysis

Statistical analysis was performed using SPSS for Windows (18.0, 2010, SPSS, Inc., Chicago, IL). We used the Shapiro-Wilk test to examine the normality of the data and found our data were normally distributed. Therefore, mixed model analysis and Benjamini-Hochberg post hoc analysis were used to access the differences caused by drug application and recording location. Statistical significance was determined at $P < .05$. Data were presented as mean ± SE.

RESULTS

We implanted a single electrode in the PFC and 4 electrodes in the AC on the left-brain hemisphere of 22 mice. Multiple electrodes were used in the AC to collect more spike activities, and the LFP signal averaged across the 4 electrodes was used as the LFP of AC. Stable signal could not be collected in the PFC of 6 mice and in the AC of 2 mice due to the unsuccessful surgery of electrode implantation. In these 8 mice, we collected data from only the AC or the PFC. The recording experiments were repeated 4 times for each mouse; in total, 80 sessions (20×4) of data were collected in the AC and 64 sessions (16×4) in the PFC. Sixteen and 8 sessions were excluded in the data of the AC and PFC, respectively, because the occurrence frequency of moving

artifacts was higher than 5%. There was no correlation between the number of discarded session and drug application. As a result, we successfully acquired 64 LFP data sets in the AC (34 of MK-801 injection, 30 of vehicle injection) and 56 in the PFC (30 of MK-801 injection, 26 of vehicle injection). The representative examples of LFPs in AC averaged over 120 trials of 40-Hz click-train stimulus are presented in Figure 1. Before the injection (Pre), click-train stimuli evoked a large deflection at the stimulus onset in the LFP of AC, and a stable oscillation of LFP synchronizing to each click stimulus was observed during the stimulus period (Figure 1A,C). To compare with the repetition rate of click stimulus, the LFPs were filtered with a bandpass filter of 35–45 Hz (Figure 1A,C, lower panel). The filtered LFP showed an obvious oscillation during the stimulus period, and the amplitude of oscillation was steady during the stimulus period (ASSR). Injection of vehicle did not obviously affect the click-train evoked responses (Figure 1B). In contrast, MK-801 injection obviously suppressed the ASSR, while the onset response was less affected (Figure 1D).

The representative examples of LFPs in the PFC are presented in Figure 2. Click-train stimuli only evoked a clear onset response of LFP in the PFC; ASSR during the stimulus period was too weak to be robustly evaluated (Figure 2A,C). Injection of vehicle or MK-801 injection had no obvious effect on the LFP response in the PFC (Figure 2B,D).

We used time-frequency analysis of the MTP and PLF to quantitatively evaluate the change of LFP. MTP reveals the amplitude of the evoked LFP, and PLF examines the trial-to-trial dynamics of the phase-locked response. The time-frequency plots of MTP and PLF at before and after vehicle/MK-801 injection are shown in Figures 3 and 4. Consistent with above inspection in Figures 1 and 2, click-trains evoked a transient increase of MTP and PLF over a broad frequency range in both AC and PFC, while only AC showed a steady increase of MTP and PLF around the 40-Hz stimulation frequency. Injection of MK-801 did not affect the onset MTP and PLF but suppressed the steady MTP and PLF in the AC (Figure 3C,D).

To compare the population results of different brain regions, we calculated the mean MTP and PLF averaged across 2 different time-frequency ranges: 0–0.1 seconds and 0–80 Hz to evaluate the onset response and 0.1–0.5 seconds and 35–45 Hz to evaluate 40 Hz ASSR (Figure 3A, white rectangles). The MTPs of the onset response in each group are presented in Figure 5A. The data were statistically analyzed with 4-factor fix model analysis: drug (MK-801 vs vehicle) × time (pre vs post) × location (AC vs PFC) × repetition (4 times of recording). No significant difference was found in the main effects and their interactions. The PLFs of the onset response in each group were similar too (Figure 5B). However, for the MTPs of the steady response (Figure 5C), a fix model analysis revealed significant differences in main effects of location ($F_{(1,208)}=850.7$; $P<.001$) and drug ($F_{(1,208)}=16.5$; $P<.001$), interaction of time × location ($F_{(1,208)}=7.7$; $P=.006$), drug × location ($F_{(1,208)}=18.4$; $P<.001$), and interaction of drug × time × location ($F_{(1,208)}=18.4$; $P<.001$). A Benjamini-Hochberg post hoc analysis revealed that the mean MTP of post MK-801 injection in the AC was significantly lower than that of pre MK-801 injection ($t=6.2$, $P<.001$). The PLFs of the steady response (Figure 5D) were also affected by location ($F_{(1,208)}=336.4$; $P<.001$) and interaction of drug × time ($F_{(1,208)}=7.6$; $P=.006$), drug × location ($F_{(1,208)}=5.9$; $P=.016$), time × location ($F_{(1,208)}=6.1$; $P=.014$), and interaction of drug × time × location ($F_{(1,208)}=14.2$; $P<.001$). A Benjamini-Hochberg post hoc analysis revealed a significant difference between the mean PLFs of the pre and post MK-801 injection group in the AC ($t=5.7$; $P<.001$).

To further reveal the neural mechanism of the MK-801–induced changes of ASSR, we examined the effect of MK-801 injection in the MGB on the spike activity of AC neurons. Figure 6 shows the raster plot and PSTH of the representative AC units. Before injection, the 40-Hz click trains evoked a repetitive firing activity with an adaptation (Figures 6A,C). The PSTH showed a peak of firing rate at the onset of stimulus and a decayed tail extending to the stimulus offset. Injection of vehicle had no significant effect on the neural firing activity (Figure 6B), while injection of MK-801 reduced the firing activity during the steady stimulus period. We

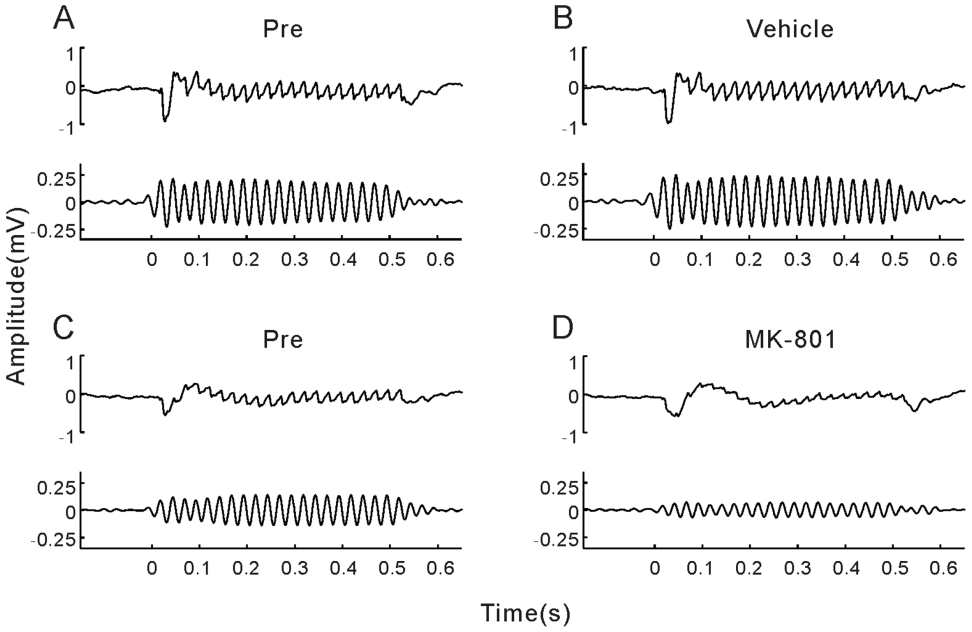

Figure 1. Examples of click-train evoked local field potentials (LFPs) recorded from the auditory cortex (AC). (A,B) LFPs recorded before and after injection of vehicle. Top panel: unfiltered LFP averaged from 120 trials of electroencephalographic (EEG) signals evoked by 40-Hz click stimuli lasting from 0 to 0.5 seconds. Bottom panel: the same EEG responses filtered with a bandpass filter. (C,D) LFPs recorded before and after injection of MK-801.

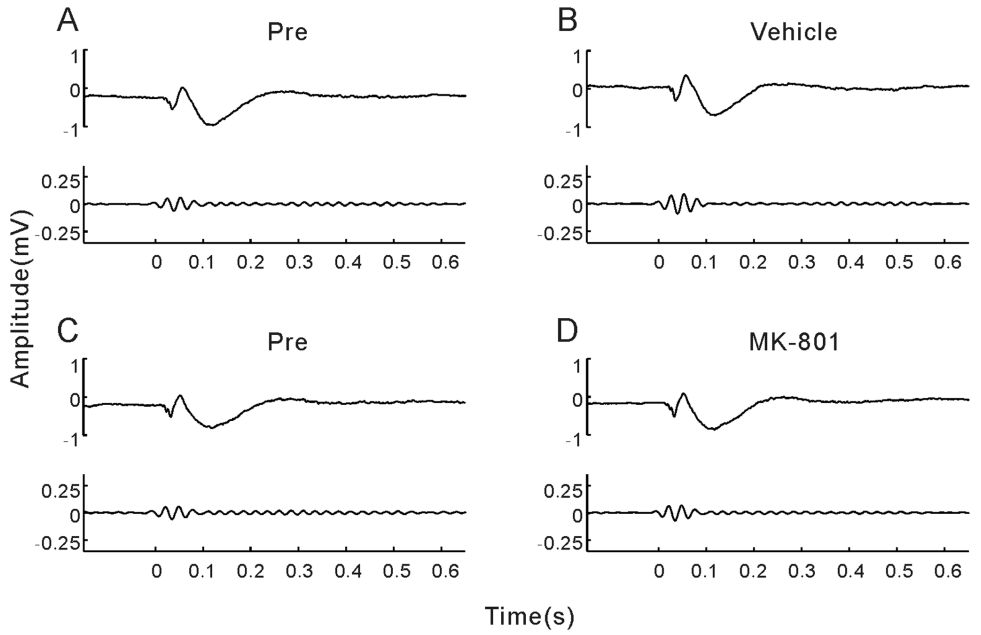

Figure 2. Examples of click-train evoked LFPs recorded from the prefrontal cortex (PFC) and using the same format as Figure 1.

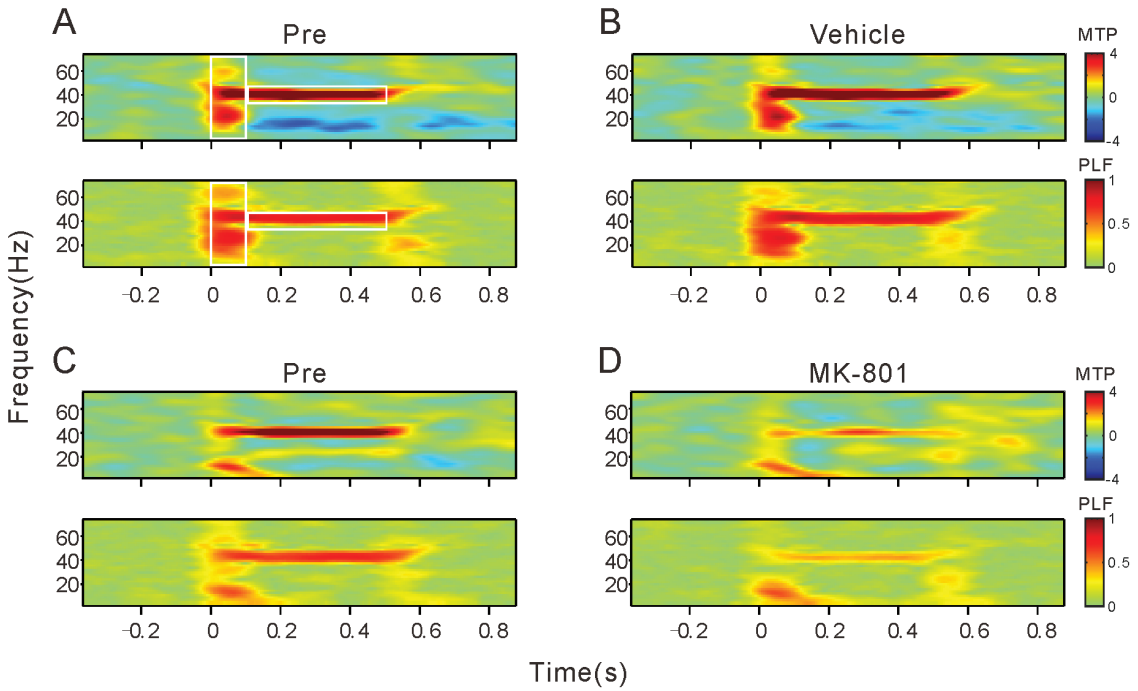

Figure 3. Spectral-temporal analysis of the example LFPs shown in Figure 1. (A,B) before and after injection of vehicle. Top panel: spectral-temporal function of main trial power (MTP). Bottom panel: spectral-temporal function of phase-locking factor (PLF). White rectangles show the time-frequency ranges: 0–0.1 seconds and 0–80 Hz to evaluate the onset response; and 0.1–0.5 seconds and 35–45 Hz to evaluate 40 Hz ASSR. (C,D) Before and after injection of MK-801.

calculated the mean firing rates during the –0.5–0, 0–0.1, and 0.1–0.5 second time window to evaluate the spontaneous activity, the onset, and steady response, respectively. Figure 7 shows the mean and SE of firing rate of AC units during different time windows. A fixed model analysis did not find any significant differences in the spontaneous activities (Figure 7A) and the onset responses (Figure 7B), but a significant mean effect of drug ($F_{(1,80)}$=11.3, P=.001) and interaction of drug×time ($F_{(1,80)}$=6.2, P=.015) was found in the steady responses (Figure 7C). A Benjamini-Hochberg post hoc analysis confirmed that the steady responses in the post MK-801 injection were significantly lower than those in the pre MK-801 injection (t=2.8; P=.044).

Discussion

ASSR, as an evoked gamma band oscillation, provides an approach for examining the synchronized responses from large ensembles of neurons and binding neural activity across brain

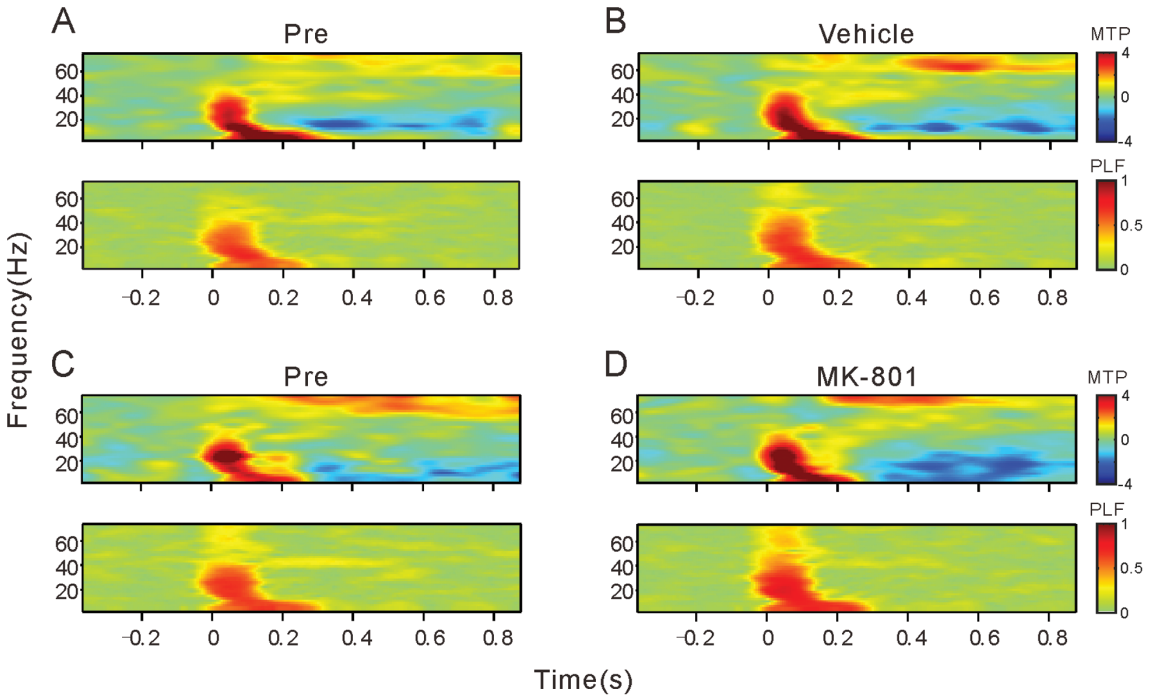

Figure 4. Spectral-temporal analysis of the example LFPs shown in Figure 2 and using the same format as Figure 3.

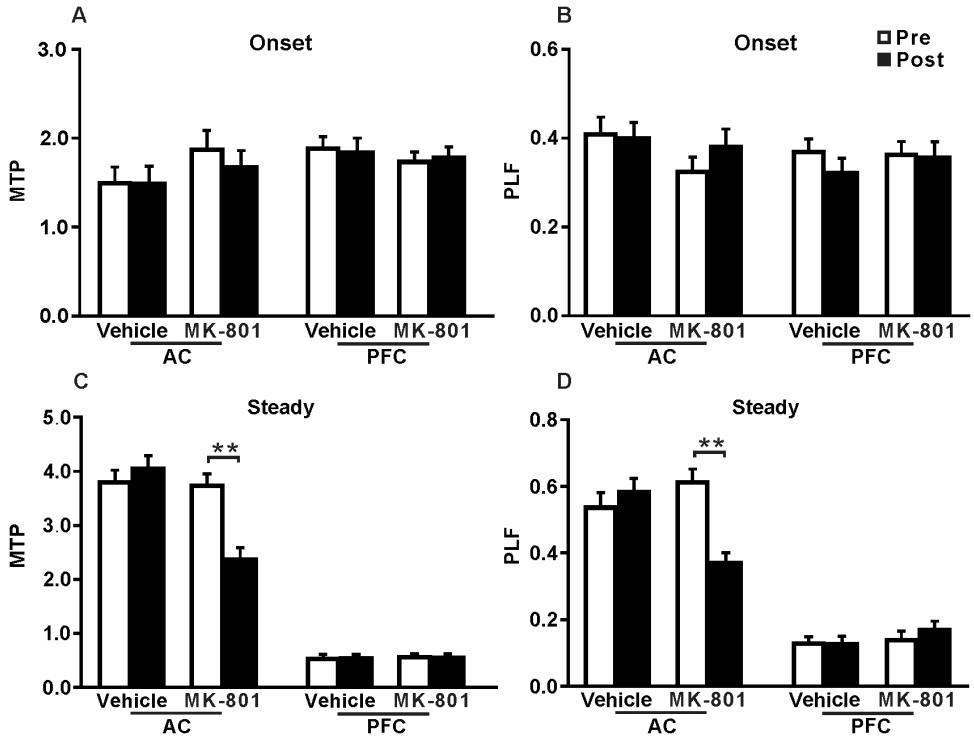

Figure 5. Mean MTP and PLF of the onset and steady response under different conditions. Bars represent the mean and SE. **P < .01.

areas (Pastor et al., 2002; Picton et al., 2003; Uhlhaas et al., 2010). Also, some studies on humans suggest that 40-Hz ASSR reflects some resonant responses generated by the superposition of the auditory brainstem response and middle latency responses that are specifically enhanced during 40-Hz stimulation (Bohórquez et al., 2008; Presacco et al., 2010). In the present study, we attempted to identify how ASSR was altered in a model of NMDAR hypofunction. For this, we recorded click-train evoked LFPs and spike activities from the AC and PFC of awake mice before and after intrageniculate injection of MK-801. We found that 40-Hz click-trains evoked a transient LFP response at the onset of stimulus and a steady response during the steady

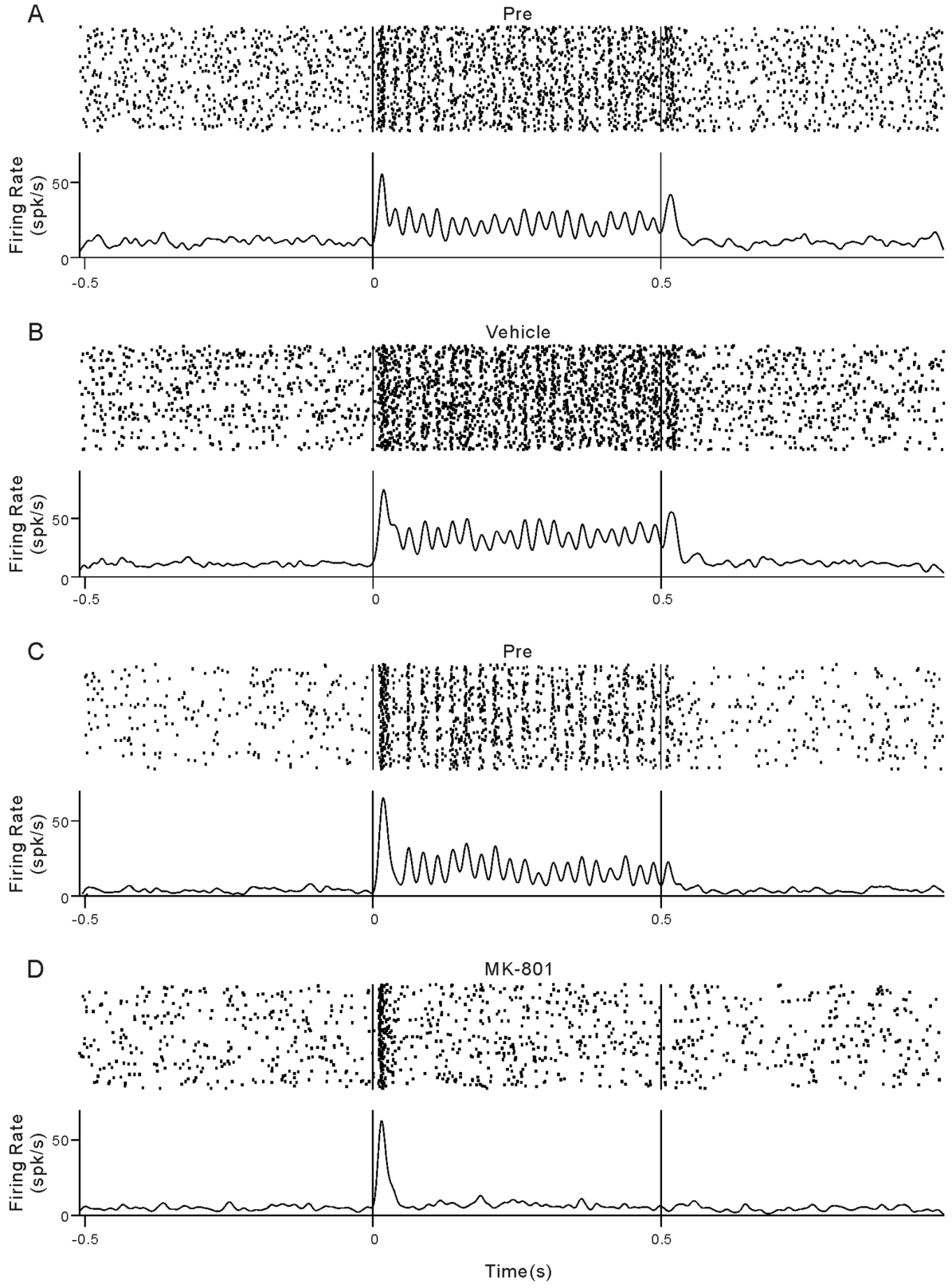

Figure 6. Examples of spike activity in the AC. (A,B) Spike activity recorded before and after injection of vehicle. Top panel: raster displays of spike discharges. Bottom panel: peristimulus time histograms (PSTHs) constructed from the raster displays. Vertical lines mark the onset of conditioning and testing tones. (C,D) Spike activity recorded before and after injection of MK-801.

period of stimulus (ASSR). The onset responses were observed in both the AC and PFC, while the ASSRs were only found in the AC. Microinjection of MK-801 (1.5 μg) into the MGB significantly suppressed the ASSR in the AC but did not affect the onset responses in the AC and PFC. The firing pattern of AC neurons showed a similar change as the LFP.

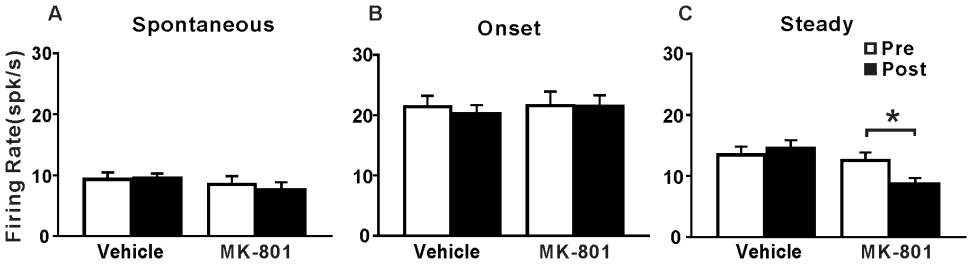

Figure 7. Mean firing rate of the spontaneous activity, onset, and steady response under different conditions. Bars represent mean and SE. *P < .05.

There is accumulating evidence showing that power or phase synchronization of 40-Hz ASSRs is reduced in SZ patients (Spencer et al., 2009; Hamm et al., 2011; Mulert et al., 2011; Tsuchimoto et al., 2011; Koenig et al., 2012; Hirano et al., 2015) and individuals vulnerable to SZ (Rass et al., 2012). The deficits of 40-Hz ASSR may reflect the hypofunction of NMDAR (Sivarao et al., 2016), which has been hypothesized to contribute to the pathophysiology of SZ (Javitt et al., 2012; Moghaddam et al., 2012). Administration of NMDAR antagonists can elicit transient schizophrenic-like positive and negative symptoms in humans and produce schizophrenia-related phenotypes in rodents (Gandal et al., 2012; Moghaddam et al., 2012). In this way, NMDAR antagonists were used in rodents to test whether alterations in NMDAR function produce electrophysiological disturbances similar to those observed in patients with SZ (Vohs et al., 2012; Hiyoshi et al., 2014; Leishman et al., 2015; Sullivan et al., 2015; Kozono et al., 2019). However, the results showed a profound impact of NMDAR antagonists on the ASSR, which was inconsistent with the observations in SZ patients. The effect of NMDAR antagonist on ASSR may differ by brain region and local neural architecture. A strength of our approach in mice is that we had the ability to record LFP signals simultaneously from multiple brain areas during the ASSR in unrestrained mice. This enabled us to probe the generation and transmission of ASSR within the mouse brain. Furthermore, we could directly administrate MK-801 to the MGB, avoiding the potential side effects of systemic administration of NMDAR antagonist. Our results showed that the click-train evoked responses have 2 segments in the temporal domain: onset response and ASSR. Previous studies on the neural spike activities have also revealed 2 temporal patterns of discharge in the auditory neurons of awake animals (Qin et al., 2004; Wang et al., 2005; Ma et al., 2013): one is the transient response phase-locking to the onset of sound stimulus, and the other is the sustained response continuing throughout the stimulus period. Our spike data recorded in the AC also showed a similar result. The new finding in the present study is that the onset response was observed in both the PFC and the AC, while the ASSR was found only in the AC, suggesting that the onset signal of a sound stimulus can be broadly transmitted among the brain, whereas the transmission of steady sound signals was localized in the auditory system. More importantly, we found that blocking the NMDAR in the MGB can easily cause a significant decrease of ASSR in the AC. In contrast, the onset responses in the AC and PFC are not changed by the blockade of NMDAR in the MGB. These results confirmed that the ASSR in the AC originate from the glutamatergic activity in the MGB, while the onset response in the AC and PFC may have multiple originators not dependent on the NMDAR neurons in the MGB. The distinct characteristics of the onset response and ASSR may be associated with the differences between their functions. The transient and widespread onset response may serve as an alert signal for an external acoustic event, while the sustained and localized response may be responsible for capturing and encoding the ethological referents contained in the sounds (Wang et al., 2005).

Resting-state functional magnetic resonance imaging connectivity studies in humans have provided broad support to abnormal functional interactions between the cortex and thalamus in SZ (Gupta et al., 2009; Minzenberg et al., 2009; Welsh et al., 2010). A specific disruption of synaptic transmission at thalamocortical projections in the AC was also found in murine models of SZ (Chun et al., 2014). In this study, we found that disrupting the NMDAR function in MGB can cause a reduction of ASSR in the AC similar to the demonstrations of SZ patients. Our findings provide the evidence suggesting that ASSR deficits in SZ may be related to NMDAR dysfunction at the level of thalamocortical connectivity. This is in agreement with the NMDAR-hypofunction hypothesis in SZ (Nakazawa et al., 2020). Postmortem studies have consistently provided molecular evidence for NMDAR-hypofunction in SZ and found that NMDAR expression levels are reduced in the thalamus (Meador-Woodruff et al., 2003).

Because functional magnetic resonance imaging studies showed increased functional connectivity between the thalamus and sensory cortex in SZ patients (Welsh et al., 2010; Woodward et al., 2012; Anticevic et al., 2015), this raises the question of how blockage of NMDAR in the MGB could lead to increased thalamocortical connectivity. A possible explanation is that MK-801 may primarily work on the NMDAr in GABAergic interneurons and suppress their inhibitory activities, whereas the excitatory activities from pyramidal neurons increased by disinhibition. It has been established that synaptic interactions between GABAergic interneurons and pyramidal neurons determine the excitation/inhibition balance in neural circuit functioning and contribute to the generation of gamma oscillations (Cardin et al., 2009; Sohal et al., 2009). There is also evidence that NMDARs contribute more to the excitatory postsynaptic currents in GABAergic interneurons than in pyramidal neurons (Jones et al., 1993), and ketamine/MK-801 preferentially blocks NMDARs in GABAergic interneurons (Homayoun et al., 2007; Suryavanshi et al., 2014; Fan et al., 2018). Thus, it is important to further examine the hypothesis that GABAergic interneurons are particularly affected by NMDAr hypofunction in SZ (Cohen et al., 2015). Moreover, the other unresolved question in this study is whether the abnormality of NMDAR-mediated MGB-AC communication is the specific mechanism leading to 40-Hz ASSR deficits in SZ patients. Multiple receptors of other neurotransmitters, such as $GABA_A$ receptor (Waldvogel et al., 2017) and dopamine D2/D3 receptor (Buchsbaum et al., 2006), participate in the MGB-AC communication. Whether and how they are involved in regulation of 40-Hz ASSR in AC need to be testified in future studies.

In conclusion, ASSRs appear to be highly sensitive to acute administration of an NMDAR antagonist in the MGB. As suggested

by the present data in mice and previous studies in humans, the MGB contributes to the generation of ASSR in the AC and NMDAR hypofunction is associated with the reduction of ASSR. Parallel use of ASSR paradigms in humans and rodent models thus provides a powerful translational vehicle for testing putative cellular mechanisms and development of novel treatments targeting neural circuits for understanding the effects of abuse of NMDAR antagonists and clinical syndromes affecting NMDAR function such as anti-NMDA encephalitis. Important limitations of the current study include lack of precise control of drug distribution range, lack of identification of cell types (pyramid or inter-neuron), and the use of single rather than multiple types of drugs. Future studies combined with assessment of cell type will help better characterize the cellular and circuit mechanisms of ASSR generation and elucidate the functional consequences of thalamocortical disconnectivity.

Acknowledgments

X.W. was primarily responsible for experiment procedures, data collection, and analysis; Y.L. and J.L. assisted with electrophysiological recording; J.C. and Z.L. assisted with analysis of electrophysiological data; L.Q. was primarily responsible for experimental design, data analysis, and manuscript preparation. All authors contributed to and approved of the final version of the manuscript.
This work was supported by the following grants: National Nature Science Foundation of China under grant (31671080 to L.Q.).

Interest Statement:

All authors declare no conflict of interest.

References

Anticevic A, Cole MW, Repovs G, Murray JD, Brumbaugh MS, Winkler AM, Savic A, Krystal JH, Pearlson GD, Glahn DC (2014) Characterizing thalamo-cortical disturbances in schizophrenia and bipolar illness. Cereb Cortex 24:3116–3130.

Anticevic A, et al. (2015) Association of thalamic dysconnectivity and conversion to psychosis in youth and young adults at elevated clinical risk. JAMA Psychiatry 72:882–891.

Bendor D, Wang X (2010) Neural coding of periodicity in marmoset auditory cortex. J Neurophysiol 103:1809–1822.

Blot K, Bai J, Otani S (2013) The effect of non-competitive NMDA receptor antagonist MK-801 on neuronal activity in rodent prefrontal cortex: an animal model for cognitive symptoms of schizophrenia. J Physiol Paris 107:448–451.

Blot K, Kimura S, Bai J, Kemp A, Manahan-Vaughan D, Giros B, Tzavara E, Otani S (2015) Modulation of hippocampus-prefrontal cortex synaptic transmission and disruption of executive cognitive functions by MK-801. Cereb Cortex 25:1348–1361.

Bohórquez J, Ozdamar O (2008) Generation of the 40-Hz auditory steady-state response (ASSR) explained using convolution. Clin Neurophysiol 119:2598–2607.

Buchsbaum MS, Christian BT, Lehrer DS, Narayanan TK, Shi B, Mantil J, Kemether E, Oakes TR, Mukherjee J (2006) D2/D3 dopamine receptor binding with [F-18]fallypride in thalamus and cortex of patients with schizophrenia. Schizophr Res 85:232–244.

Cardin JA, Carlén M, Meletis K, Knoblich U, Zhang F, Deisseroth K, Tsai LH, Moore CI (2009) Driving fast-spiking cells induces gamma rhythm and controls sensory responses. Nature 459:663–667.

Chun S, Westmoreland JJ, Bayazitov IT, Eddins D, Pani AK, Smeyne RJ, Yu J, Blundon JA, Zakharenko SS (2014) Specific disruption of thalamic inputs to the auditory cortex in schizophrenia models. Science 344:1178–1182.

Cohen SM, Tsien RW, Goff DC, Halassa MM (2015) The impact of NMDA receptor hypofunction on GABAergic neurons in the pathophysiology of schizophrenia. Schizophr Res 167:98–107.

Delorme A, Makeig S (2004) EEGLAB: an open source toolbox for analysis of single-trial EEG dynamics including independent component analysis. J Neurosci Methods 134:9–21.

Dong C, Qin L, Liu Y, Zhang X, Sato Y (2011) Neural responses in the primary auditory cortex of freely behaving cats while discriminating fast and slow click-trains. Plos One 6:e25895.

Dong C, Qin L, Zhao Z, Zhong R, Sato Y (2013) Behavioral modulation of neural encoding of click-trains in the primary and nonprimary auditory cortex of cats. J Neurosci 33:13126–13137.

Fan LZ, Nehme R, Adam Y, Jung ES, Wu H, Eggan K, Arnold DB, Cohen AE (2018) All-optical synaptic electrophysiology probes mechanism of ketamine-induced disinhibition. Nat Methods 15:823–831.

Gandal MJ, Edgar JC, Klook K, Siegel SJ (2012) Gamma synchrony: towards a translational biomarker for the treatment-resistant symptoms of schizophrenia. Neuropharmacology 62:1504–1518.

Giraldo-Chica M, Woodward ND (2017) Review of thalamocortical resting-state fMRI studies in schizophrenia. Schizophr Res 180:58–63.

Gupta A, Bhakta S, Kundu S, Gupta M, Srivastava BS, Srivastava R (2009) Fast-growing, non-infectious and intracellularly surviving drug-resistant Mycobacterium Aurum: a model for high-throughput antituberculosis drug screening. J Antimicrob Chemother 64:774–781.

Gutschalk A, Mase R, Roth R, Ille N, Rupp A, Hähnel S, Picton TW, Scherg M (1999) Deconvolution of 40 Hz steady-state fields reveals two overlapping source activities of the human auditory cortex. Clin Neurophysiol 110:856–868.

Hamm JP, Gilmore CS, Picchetti NA, Sponheim SR, Clementz BA (2011) Abnormalities of neuronal oscillations and temporal integration to low- and high-frequency auditory stimulation in schizophrenia. Biol Psychiatry 69:989–996.

Herdman AT, Lins O, Van Roon P, Stapells DR, Scherg M, Picton TW (2002) Intracerebral sources of human auditory steady-state responses. Brain Topogr 15:69–86.

Hirano Y, Oribe N, Kanba S, Onitsuka T, Nestor PG, Spencer KM (2015) Spontaneous gamma activity in schizophrenia. JAMA Psychiatry 72:813–821.

Hiyoshi T, Kambe D, Karasawa J, Chaki S (2014) Involvement of glutamatergic and GABAergic transmission in MK-801-increased gamma band oscillation power in rat cortical electroencephalograms. Neuroscience 280:262–274.

Homayoun H, Moghaddam B (2007) NMDA receptor hypofunction produces opposite effects on prefrontal cortex interneurons and pyramidal neurons. J Neurosci 27:11496–11500.

Javitt DC, Zukin SR, Heresco-Levy U, Umbricht D (2012) Has an angel shown the way? Etiological and therapeutic implications of the PCP/NMDA model of schizophrenia. Schizophr Bull 38:958–966.

Jones RS, Bühl EH (1993) Basket-like interneurones in layer II of the entorhinal cortex exhibit a powerful NMDA-mediated synaptic excitation. Neurosci Lett 149:35–39.

Kirov G, et al. (2012) De novo CNV analysis implicates specific abnormalities of postsynaptic signalling complexes in the pathogenesis of schizophrenia. Mol Psychiatry 17:142–153.

Klingner CM, Langbein K, Dietzek M, Smesny S, Witte OW, Sauer H, Nenadic I (2014) Thalamocortical connectivity during resting state in schizophrenia. Eur Arch Psychiatry Clin Neurosci 264:111–119.

Koenig T, van Swam C, Dierks T, Hubl D (2012) Is gamma band EEG synchronization reduced during auditory driving in schizophrenia patients with auditory verbal hallucinations? Schizophr Res 141:266–270.

Kozono N, Honda S, Tada M, Kirihara K, Zhao Z, Jinde S, Uka T, Yamada H, Matsumoto M, Kasai K, Mihara T (2019) Auditory Steady State response; nature and utility as a translational science tool. Sci Rep 9:8454.

Leishman E, O'Donnell BF, Millward JB, Vohs JL, Rass O, Krishnan GP, Bolbecker AR, Morzorati SL (2015) Phencyclidine disrupts the auditory steady state response in rats. Plos One 10:e0134979.

Ma L, Tai X, Su L, Shi L, Wang E, Qin L (2013) The neuronal responses to repetitive acoustic pulses in different fields of the auditory cortex of awake rats. Plos One 8:e64288.

Malmierca MS (2003) The structure and physiology of the rat auditory system: an overview. Int Rev Neurobiol 56:147–211.

McNally JM, McCarley RW (2016) Gamma band oscillations: a key to understanding schizophrenia symptoms and neural circuit abnormalities. Curr Opin Psychiatry 29:202–210.

Meador-Woodruff JH, Clinton SM, Beneyto M, McCullumsmith RE (2003) Molecular abnormalities of the glutamate synapse in the thalamus in schizophrenia. Ann N Y Acad Sci 1003:75–93.

Minzenberg MJ, Laird AR, Thelen S, Carter CS, Glahn DC (2009) Meta-analysis of 41 functional neuroimaging studies of executive function in schizophrenia. Arch Gen Psychiatry 66:811–822.

Moghaddam B, Krystal JH (2012) Capturing the angel in "angel dust": twenty years of translational neuroscience studies of NMDA receptor antagonists in animals and humans. Schizophr Bull 38:942–949.

Mulert C, Kirsch V, Pascual-Marqui R, McCarley RW, Spencer KM (2011) Long-range synchrony of γ oscillations and auditory hallucination symptoms in schizophrenia. Int J Psychophysiol 79:55–63.

Nakazawa K, Sapkota K (2020) The origin of NMDA receptor hypofunction in schizophrenia. Pharmacol Ther 205:107426.

Pastor MA, Artieda J, Arbizu J, Marti-Climent JM, Peñuelas I, Masdeu JC (2002) Activation of human cerebral and cerebellar cortex by auditory stimulation at 40 Hz. J Neurosci 22:10501–10506.

Picton TW, John MS, Dimitrijevic A, Purcell D (2003) Human auditory steady-state responses. Int J Audiol 42:177–219.

Presacco A, Bohórquez J, Yavuz E, Özdamar Ö (2010) Auditory steady-state responses to 40-Hz click trains: relationship to middle latency, gamma band and beta band responses studied with deconvolution. Clin Neurophysiol 121:1540–1550.

Qin L, Sato Y (2004) Suppression of auditory cortical activities in awake cats by pure tone stimuli. Neurosci Lett 365:190–194.

Rass O, Forsyth JK, Krishnan GP, Hetrick WP, Klaunig MJ, Breier A, O'Donnell BF, Brenner CA (2012) Auditory steady state response in the schizophrenia, first-degree relatives, and schizotypal personality disorder. Schizophr Res 136:143–149.

Sivarao DV, Chen P, Senapati A, Yang Y, Fernandes A, Benitex Y, Whiterock V, Li YW, Ahlijanian MK (2016) 40 Hz auditory steady-state response is a pharmacodynamic biomarker for cortical NMDA receptors. Neuropsychopharmacology 41:2232–2240.

Sohal VS, Zhang F, Yizhar O, Deisseroth K (2009) Parvalbumin neurons and gamma rhythms enhance cortical circuit performance. Nature 459:698–702.

Spencer KM, Niznikiewicz MA, Nestor PG, Shenton ME, McCarley RW (2009) Left auditory cortex gamma synchronization and auditory hallucination symptoms in schizophrenia. BMC Neurosci 10:85.

Stefani MR, Moghaddam B (2005) Systemic and prefrontal cortical NMDA receptor blockade differentially affect discrimination learning and set-shift ability in rats. Behav Neurosci 119:420–428.

Sullivan EM, Timi P, Hong LE, O'Donnell P (2015) Effects of NMDA and GABA-A receptor antagonism on auditory steady-state synchronization in awake behaving rats. Int J Neuropsychopharmacol 18:pyu118.

Suryavanshi PS, Ugale RR, Yilmazer-Hanke D, Stairs DJ, Dravid SM (2014) GluN2C/GluN2D subunit-selective NMDA receptor potentiator CIQ reverses MK-801-induced impairment in prepulse inhibition and working memory in Y-maze test in mice. Br J Pharmacol 171:799–809.

Tada M, Kirihara K, Koshiyama D, Fujioka M, Usui K, Uka T, Komatsu M, Kunii N, Araki T, Kasai K (2019) Gamma-band auditory steady-state response as a neurophysiological marker for excitation and inhibition balance: a review for understanding schizophrenia and other neuropsychiatric disorders. Clin EEG Neurosci. doi: 10.1177/1550059419868872.

Thuné H, Recasens M, Uhlhaas PJ (2016) The 40-Hz auditory steady-state response in patients with schizophrenia: a meta-analysis. JAMA Psychiatry 73:1145–1153.

Timms AE, Dorschner MO, Wechsler J, Choi KY, Kirkwood R, Girirajan S, Baker C, Eichler EE, Korvatska O, Roche KW, Horwitz MS, Tsuang DW (2013) Support for the N-methyl-D-aspartate receptor hypofunction hypothesis of schizophrenia from exome sequencing in multiplex families. JAMA Psychiatry 70:582–590.

Tsuchimoto R, Kanba S, Hirano S, Oribe N, Ueno T, Hirano Y, Nakamura I, Oda Y, Miura T, Onitsuka T (2011) Reduced high and low frequency gamma synchronization in patients with chronic schizophrenia. Schizophr Res 133:99–105.

Uhlhaas PJ, Singer W (2010) Abnormal neural oscillations and synchrony in schizophrenia. Nat Rev Neurosci 11:100–113.

Umbricht D, Schmid L, Koller R, Vollenweider FX, Hell D, Javitt DC (2000) Ketamine-induced deficits in auditory and visual context-dependent processing in healthy volunteers: implications for models of cognitive deficits in schizophrenia. Arch Gen Psychiatry 57:1139–1147.

Vohs JL, Chambers RA, O'Donnell BF, Krishnan GP, Morzorati SL (2012) Auditory steady state responses in a schizophrenia rat model probed by excitatory/inhibitory receptor manipulation. Int J Psychophysiol 86:136–142.

Waldvogel HJ, Munkle M, van Roon-Mom W, Mohler H, Faull RLM (2017) The immunohistochemical distribution of the GABAA receptor α1, α2, α3, β2/3 and γ2 subunits in the human thalamus. J Chem Neuroanat 82:39–55.

Wang X, Lu T, Snider RK, Liang L (2005) Sustained firing in auditory cortex evoked by preferred stimuli. Nature 435:341–346.

Wang Y, Ma L, Wang X, Qin L (2018) Differential modulation of the auditory steady state response and inhibitory gating by chloral hydrate anesthesia. Sci Rep 8:3683.

Welsh RC, Chen AC, Taylor SF (2010) Low-frequency BOLD fluctuations demonstrate altered thalamocortical connectivity in schizophrenia. Schizophr Bull 36:713–722.

Woodward ND, Karbasforoushan H, Heckers S (2012) Thalamocortical dysconnectivity in schizophrenia. Am J Psychiatry 169:1092–1099.